Deconvoluting Sources of Failure in Lithium Metal Batteries Containing NMC and PEO-Based Electrolytes

W. Blake Hawley[1,2], Zhijia Du[1], Alexander J. Kukay[1,2], Nancy J. Dudney[3], Andrew S. Westover[3], Jianlin Li[1,2*]

[1]Electrification and Energy Infrastructures Division, Oak Ridge National Laboratory, Oak Ridge, TN USA 37831

[2]University of Tennessee, Bredesen Center for Interdisciplinary Research and Graduate Education, Knoxville, TN USA 37996

[3]Chemical Sciences Division, Oak Ridge National Laboratory, Oak Ridge, TN USA 37831

Abstract

Solid-state lithium metal batteries (SSLMBs) containing polyethylene oxide (PEO)-derived polymer electrolytes and high-voltage (> 4 V vs. Li/Li^+) cathode materials suffer from three sources of failure: (1) instability between the polymer electrolyte and cathode at high voltage, (2) instability of the polymer electrolyte with Li metal, and (3) poorly-designed cathodes. In this study, these three sources of failure are deconvoluted by studying Ni-rich $LiNi_xMn_yCo_{1-x-y}O_2$ (NMC, $x \geq 0.6$) cathodes and a gel polymer electrolyte (GPE) derived from PEO. Initial cycling data reveals that rapid capacity fade occurs regardless of whether soft short circuits form due to Li dendrites. Cyclic voltammetry scans on cells featuring a Li metal electrode, GPE, and a NMC811 electrode free of additives suggest that there are no runaway reactions between the GPE and NMC811 up to 4.5 V vs. Li/Li^+. Cathode/cathode symmetric cell cycling demonstrates that Li metal reactivity is a prime source of failure, though a poorly-designed cathode leads to subpar performance. A

cathode with single-crystal NMC particles was demonstrated to achieve better initial capacity and longer cycle life, indicating room for improvement in SSLMB cathode design. Therefore, the sources of failure as enumerated may be ranked as follows from most to least concerning: 2 > 3 > 1.

Keywords: solid-state battery, high-voltage cathode, dust electrode, cyclic voltammetry, symmetric cell, single-crystal cathode

*Corresponding author: lij4@ornl.gov

Highlights

- Sudden, rapid capacity fade observed in cells with gel polymer electrolyte
- Cyclic voltammetry suggests good stability between NMC and gel polymer electrolyte
- Li dendrites and instability with gel polymer electrolyte are of primary concern
- Capacity fade due to cathode can be partially overcome with better cathode design

1. Introduction

Solid-state lithium metal batteries (SSLMBs) are an attractive alternative to lithium-ion batteries for improved safety [1] and energy density [2] purposes. Polymer electrolytes are attractive choices for SSLMBs since they are among the easiest solid electrolytes to produce at scale [3] and are environmentally friendly [4]; the relative advantages and disadvantages of all solid electrolyte classes are considered elsewhere [3, 5]. The most researched polymer electrolytes generally use polyethylene oxide (PEO), or derivates thereof, due to its ability to solvate many Li salts, low density, and good contact with electrodes [6, 7].

Among the primary concerns with PEO-based polymer electrolytes is its perceived instability with high-voltage (> 4 V vs. Li/Li^+) cathode materials, such as $LiNi_xMn_yCo_{1-x-y}O_2$ (NMC). For SSLMBs to achieve their capability as energy-dense devices, this restriction essentially forbids the use of polymer electrolytes without the use of a protective coating. PEO has been reported to be unstable at oxidative potentials above 3.8 V vs. Li/Li^+ [8, 9], which would limit the cathode to low-voltage options such as $LiFePO_4$ (LFP) [6, 10]. PEO has also been used with the high-voltage material $LiCoO_2$ (LCO) [11-13]; however, in each of these studies, the LCO particles had a protective coating so that they did not make direct contact with the PEO-containing electrolyte. Contrasting these results, Homann et al. concluded that PEO was stable up to 4.6 V with a variety of cathode materials, including $LiNi_{0.6}Mn_{0.2}Co_{0.2}O_2$ (NMC622), $LiMn_2O_4$, $LiNi_{0.5}Mn_{1.5}O_4$, and LFP, from observing the galvanostatic charge curve [14]. Their work suggests that the primary problem lies with the development of "soft" short circuits that prevent the cell from charging to the upper cutoff potential within the first couple of cycles.

Based on the preceding discussion, there are at least three sources of failure that have been investigated in the literature in cells containing PEO-derived electrolytes and high-voltage

cathodes: (1) electrochemical instability between the electrolyte and cathode, (2) Li metal dendrite propagation creating a short circuit in the cell, and (3) a poorly designed cathode. This study has been designed to deconvolute these three sources of failure and grade them for a cell containing Ni-rich NMCs (Ni content ≥ 0.6) and a UV-curable gel polymer electrolyte (GPE) developed in previous work from the authors [15]. The authors used linear sweep voltammetry in a Li | GPE | stainless steel cell, which indicated that the GPE is stable up to 4.5 V vs. Li/Li^+; at higher potentials, the current increase was attributed to anodic breakdown caused by degradation of the GPE [15].

In this work, initial cycling results suggest that the cells become highly resistive within the first 40 cycles and fail to deliver much capacity shortly after the rapid capacity fade begins. To analyze the stability of NMC with the GPE, a strategy [16-18] henceforth referred to as the "dust electrode" was implemented. Dust electrodes consist of a thin layer of active materials in intimate contact with a current collector without binders and conductive additives. They have been used to obtain excellent voltammograms of many cathode active materials [16] and to calculate diffusion coefficients [18]. The dust electrode voltammograms, when combined with the cycling data, suggested that the primary issue in these cells exists at the Li metal/GPE interface. Poor cycling performance of cathode/cathode symmetric cells identified that the secondary problem is the cathode morphology, which could be alleviated by using single-crystal NMC particles. While this study cannot preclude the possibility of side reactions between NMC and PEO-derived polymers as a source of failure, it appears to be a tertiary problem compared to Li metal dendrite formation and cathode morphology.

2. Experimental

2.1 Fabrication of Electrodes and GPE

Composite cathodes were prepared by mixing 90 wt% commercially-available active material (see Table 1), 5 wt% carbon black (Denka, Li-100), and 5 wt% polyvinylidene fluoride (Solvay 5130) which was pre-mixed in N-methyl-2-pyrrolidone (NMP, Sigma Aldrich). Note that in the context of this paper, "composite" cathodes do not contain any solid electrolyte but do contain conductive additive and binder. Two types of NMC were used: polycrystalline (PC-NMC) and single-crystal (SC-NMC) particles. The cathode slurries containing PC-NMC811 and LFP were mixed in a planetary mixer (Ross, PMD – ½) and coated using a pilot-scale slot-die coater (Frontier). Due to the cost associated with purchasing large quantities of SC cathode materials, a smaller SC-NMC622 slurry was prepared in a high-energy ball mill (SPEX Sample Prep 8000M Mixer/Mill) and coated using a film applicator (Qualtech Products Industry). Images of the three cathode materials were taken using a Zeiss MERLIN^{TM} field-emission scanning electron microscope (SEM) (see Fig. S1).

Table 1. A list of commercially-available active materials used in this study.

Active Material	**Supplier**	**Diameter (d_{50}, µm)**	**Specific Surface Area ($m^2 \cdot g^{-1}$)**
PC-NMC811	Targray	13.8	0.5
SC-NMC622	MSE Supplies	3-6	0.3-0.9
LFP	Phostech Lithium Inc.	0.1	> 10

Dust electrodes were prepared by dispersing 1 wt% PC-NMC811 in acetone. Two 12.7-mm diameter discs were punched from an Au sheet (Ted Pella Inc., 99.99% purity) and a drop of

the PC-NMC811 solution was placed between them. The discs were placed in a hydraulic press and pressed at 15,000 psi. After pressing, the discs were easily separated and were washed with acetone to remove any loose particles. Embedment of the PC-NMC811 on the inward-facing disc surface was verified using a light microscope (Keyence Corp).

The GPE was prepared by mixing polyethylene glycol dimethyl ether (PEGDME, MW = 500 $g \cdot mol^{-1}$, Sigma-Aldrich), poly(ethylene glycol) diacrylate (PEGDA, MW = 575 $g \cdot mol^{-1}$, Sigma-Aldrich), and lithium bis(trifluoromethanesulfonyl)imide (LiTFSI, 3M Company) in equal parts by mass. The solution was mixed in a vortex mixer until the LiTFSI was sufficiently dispersed. Next, phenylbis(2,4,6-trimethylbenzoyl)phosphine oxide (97%, Sigma-Aldrich) was added as photoinitiator and mixed in the vortex mixer until it was well-dispersed. Once mixed, drops of the resulting gel were cured between two glass plates to control the film thickness for 2 min under a UV light source (5000-EC, Dymax Corp) [15]. The GPEs were approximately 100 μm thick for all cells tested. All electrode and GPE preparation and material storage occurred in a dry room (RH < 0.1%).

2.2 Electrochemical Measurements

All electrochemical testing was done in 2032 coin cells, which were assembled in an Ar-filled glovebox (Vigor Tech USA). Composite cathodes had an areal capacity of 0.88 ± 0.09 $mAh \cdot cm^{-2}$ (unless otherwise stated) and were galvanostatically charged and discharged at +0.1C/-0.1C at 50°C. The Li metal used as an anode in these cells was supplied by MTI Corp. (d = 16 mm, thickness = 600 μm). The areal capacity of each cell was calculated using the mass loading of active material and assuming a specific capacity of 140 $mAh \cdot g^{-1}$ for LFP, 170 $mAh \cdot g^{-1}$ for NMC622, and 185 $mAh \cdot g^{-1}$ for NMC811. Dust electrodes were studied using cyclic voltammetry

(CV) between 2.8-4.5 V starting at the open circuit potential four times at a scan rate of 0.1 $mV \cdot s^{-1}$ (unless otherwise stated). The third scan is shown in the main text, though all three scans are displayed in Fig. S2. To make symmetric cells, two composite cathodes were cycled three times at +0.1C/0.1C in separate half-cell coin cells with liquid electrolyte (LE) and separator at 30°C. Afterwards, the cells were charged to 50% state-of-charge (SOC). 50% SOC was calculated by determining the potential at which half of the total charge capacity of the third cycle had been delivered. Then, the coin cells were disassembled, and the cathodes were washed and dried before being built into a single symmetric cell with the GPE and without any LE. These symmetric cells were cycled at 50°C. For all cells containing LE, the LE used was 1.2M $LiPF_6$ in 3:7 (by weight) ethyl carbonate/ethyl methyl carbonate (Tomiyama); some cells also use Celgard separator. All cells were built with one spacer (d = 15.5 mm, thickness = 500 μm) behind both electrodes, unless otherwise specified. Cells cycled at 30°C were cycled in a reach-in testing chamber (ESPEC Inc.) and cells cycled at 50°C were cycled in a benchtop testing chamber (Cincinnati Sub-Zero).

3. Results and Discussion

3.1 Cycling Results

Galvanostatic charge/discharge experiments were performed on a SSLMB featuring PC-NMC811, GPE, and Li metal anode (see Fig. 1). The cell delivered 135.6 $mAh \cdot g^{-1}$ in its initial discharge and achieved a maximum specific discharge capacity of 140.4 $mAh \cdot g^{-1}$ in its fourth cycle, which is about 75% of the achievable specific discharge capacity of NMC811 [19]. Since the electrolyte was UV-cured prior to being built into a cell, this is likely because the electrolyte does not contact the entire cathode area. The capacity faded gradually until about the 40^{th} cycle, at which point the capacity fade increased substantially; by the 51^{st} cycle, < 10 $mAh \cdot g^{-1}$ of capacity

were delivered per discharge. The potential profile (see Fig. 1b) reveals that the cell becomes highly resistive around the 40th cycle because the slope of the charge/discharge curves increases significantly.

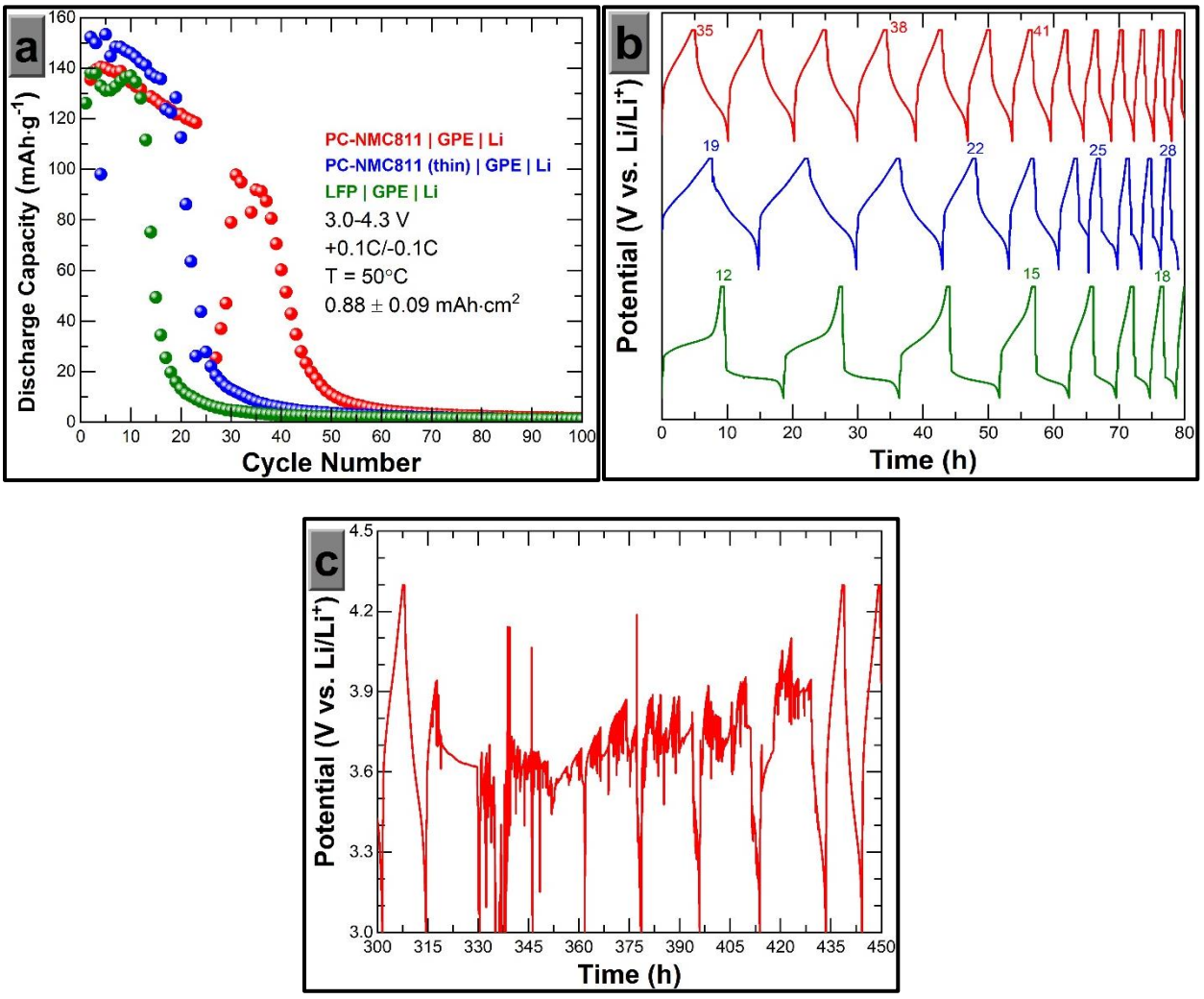

Fig. 1. a) Specific discharge capacity and b) partial potential profile of PC-NMC811 | GPE | Li (red), thin PC-NMC811 | GPE | Li (blue), and LFP | GPE | Li (green). Some cycles are labelled in the potential profile for reference. Since the three cells failed at different times, the time axis is relative. c) Partial potential profile of PC-NMC811 | GPE | Li showing the voltage noise phenomenon occurring between the 24th and 30th cycles.

Interestingly, little discharge capacity was observed between the 24th and 30th cycles due to the voltage noise phenomenon (see Fig. 1c). The voltage noise phenomenon is caused by soft short circuits developing in the cell caused by Li metal dendrite penetration [14, 20] and is not a product of unwanted side reactions between the cathode and polymer electrolyte. In this cell, the short circuit self-healed, since approximately five more cycles were completed before the onset of rapid capacity fade.

Assuming a constant porosity, electrode area, and C-rate, the thickness of a cathode correlates linearly with the areal current density. To determine if cathode thickness or current density could be causing this issue, a "thin" PC-NMC811 composite cathode was created (areal capacity = 0.59 mAh·g^{-1}). The thin cathode achieved a maximum specific discharge capacity of 153.3 mAh·g^{-1} in its fifth cycle. This improved performance could be because more cathode particles are connected to the GPE, since the PC-NMC811:GPE ratio is lower in the thin cell. Despite better initial performance, the thin PC-NMC811 cell fades just as the thicker cell did, with its rapid decline occurring around the 20th cycle.

A Ni-free, low-voltage material that has demonstrated better cyclability than NMC811 is LFP. To determine if this rapid resistance increase was caused specifically by a reaction between the NMC811 material and the GPE, a LFP | GPE | Li cell was tested at the same current density and temperature conditions. The cell delivered a maximum specific discharge capacity of 138.1 mAh·g^{-1} in its second cycle. Considering LFP is capable of about 140-170 mAh·g^{-1} depending on the quality of the dispersion of particles [19, 21, 22], this is reasonable performance. However, as with both PC-NMC811 cells, the LFP cell becomes highly resistive around the 12th cycle and fails shortly thereafter. The 100-cycle Coulombic efficiencies of the three cells were 97.4%, 97.3%,

and 98.2%, respective to the order they were discussed, which is typical of Li metal cells [23, 24] due to the high reactivity of Li [25].

3.2 Stability between NMC811 and GPE

As shown in the optical microscope images in Fig. 2, the dust electrode fabrication method outlined in Section 2.1 was successful in embedding PC-NMC811 particles onto the Au disc. The bare disc (Fig. 2a) shows only minor scratches which may come from manufacturing or material handling. The embedded disc (Fig. 2b) contains many black spots, which are the PC-NMC811 particles remaining after pressing.

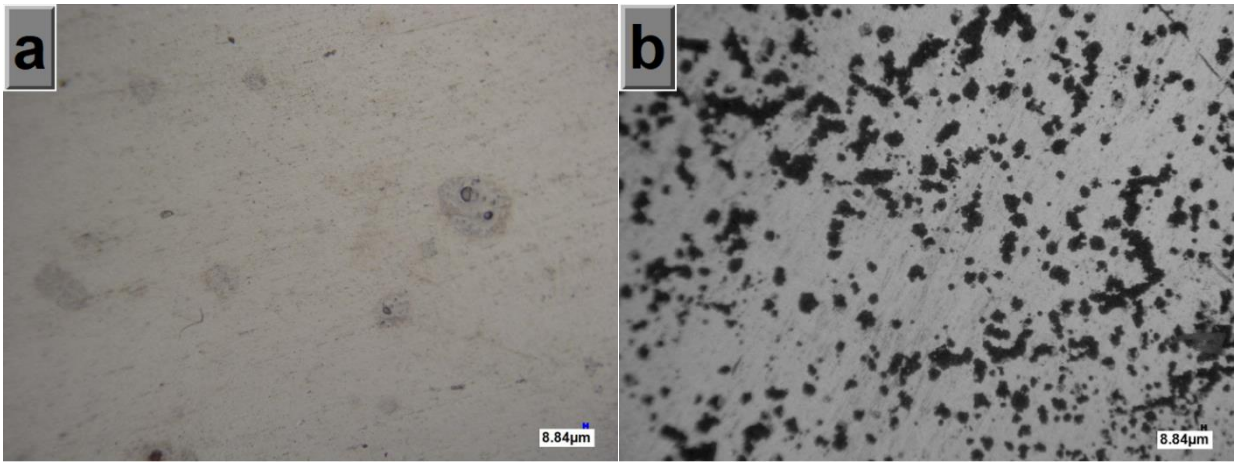

Fig. 2. a) Optimal microscope images of a) a pristine Au disc and b) a PC-NMC811 dust electrode after pressing.

To confirm the viability of the dust electrode strategy, a dust electrode was built into a coin cell with LE, separator, and Li metal anode (see Fig. 3a). There are four distinct peaks in both the forward (3.637 V, 3.739 V, 4.017 V, and 4.204 V) and reverse (3.617 V, 3.725 V, 3.991 V, and 4.181 V) scans. When counting the peaks in the forward scan, the first two peaks are caused by

the transition from a hexagonal phase (H_1) to a monoclinic phase (M). The third and fourth peaks are attributable to the transition from M to a second hexagonal phase (H_2) and the transition from H_2 to a third hexagonal phase (H_3). The first two peaks also represent the Ni^{2+}/Ni^{3+} and Ni^{3+}/Ni^{4+} redox pairs, respectively. It is rare for the individual Ni^{2+}/Ni^{3+} and Ni^{3+}/Ni^{4+} redox pairs to be observed in CV scans of NMC811, since they are commonly seen as one broad, less-resolved peak due to resistances attributable to electrode additives and/or processing conditions [26, 27]. To the best knowledge of the authors, four distinct peaks of NMC811 have only been reported in differential capacity analysis [28]. The following characteristics of a dust electrode may cause these well-resolved voltammograms when using LE and separator: (1) Intimate contact between the active material and the Au current collector, achieved by pressing them together at high pressures in the hydraulic press, (2) The thinness of the layer of active material particles on the surface of the Au current collector, and (3) The removal of binding polymers that may obstruct electron transfer.

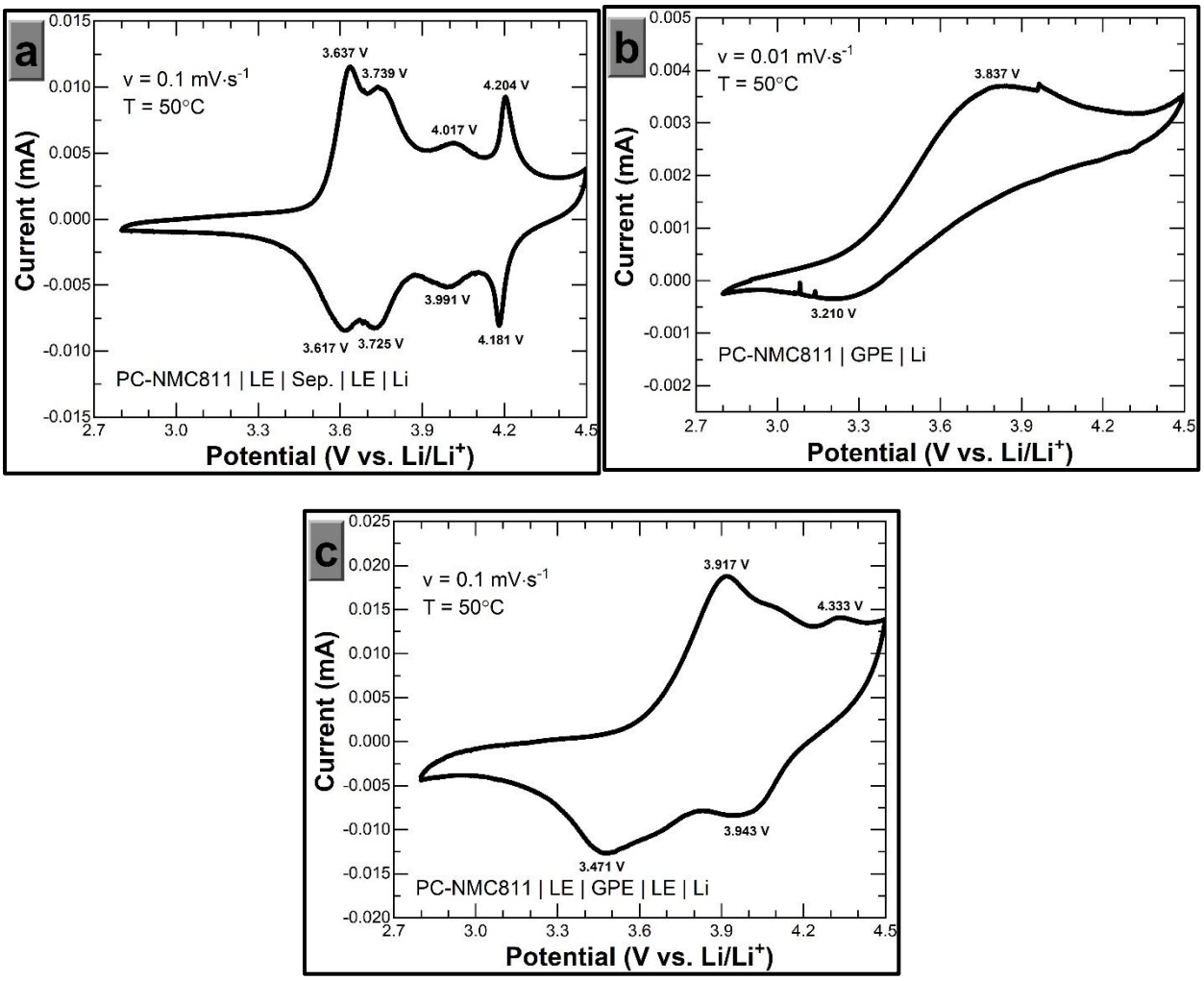

Fig. 3. a) CV of a dust electrode with LE and separator. b) CV of a dust electrode with no LE and GPE. c) CV of a dust electrode with one drop of LE on each side of the GPE. The third cycle is shown for each cell; Fig. S2 shows all three cycles for each cell.

With the dust electrode established as an analytical tool for redox processes, a dust electrode was built into a coin cell with GPE and no LE or separator (see Fig. 3b). Preliminary investigations using a scan rate of 0.1 $mV \cdot s^{-1}$ revealed no redox behavior, so a lower scan rate (0.01 $mV \cdot s^{-1}$) was used. Furthermore, an additional spacer was added to the coin cell to increase contact between the GPE and the cathode materials of the dust electrode. Even with these

modifications, just one redox peak was observed in the anodic (3.837 V) and the cathodic scan (3.210 V). Obviously, these peaks are poorly resolved and have a significant peak-to-peak separation of about 600 mV. This poor voltammogram is a product of extremely high interfacial resistance.

To overcome the high resistance, one drop of LE was added to the surfaces of the dust electrode and the Li metal anode. The drop was lightly wiped since the GPE curls when exposed to LE. This cell was built with only two spacers and was studied at 0.1 $mV \cdot s^{-1}$ (see Fig. 3c). In this scan, two peaks are seen in the forward (3.917 V and 4.333 V) and reverse (3.471 V and 3.943 V) directions. Though unmarked in the figure, a shoulder is also observed in both directions between these two peaks at approximately 4.1 V and 3.7 V, respectively. These peak-to-peak separations are about 400 mV which still suggests high cell resistance between the cathode and GPE. The fact that four distinct peaks cannot be deconvoluted is also a product of high cell resistance. High resistance is known to be a problem between cathodes and this GPE. Du et al. showed that a NMC622 | GPE | Li cell with areal capacity 0.5 $mAh \cdot cm^{-2}$ cycled between 3.0-4.3 V at 50°C and +0.1C/-0.1C achieved only about 118 $mAh \cdot g^{-1}$ in its first discharge cycle and 74 $mAh \cdot g^{-1}$ in its 30^{th} discharge cycle [15]. These low capacities suggest that there could be high mass transport resistance, just as the dust electrode scan does. It should be noted that discrepancies in the current recorded between dust electrodes is largely a product of differences in surface coverage of PC-NMC811 particles on the Au disc.

While the dust electrode with GPE was unable to reproduce the same voltammogram as the dust electrode flooded with LE, there do not appear to be additional peaks or runaway reactions that suggest an incompatibility between NMC811 and the GPE used. Even though there are no unrecognized redox peaks in the voltammogram with GPE, it should be emphasized that there

could still be some degradation reactions between NMC811 and the GPE; however, it can be stated that these reactions are significantly smaller in magnitude than the desired NMC redox reactions. With the relative stability of the electrolyte with the NMC cathodes demonstrated, it seems highly unlikely that the cell failure observed in Fig. 1 is primarily a function of side reactions.

3.3 Cathode Design Considerations

Thus far, instability between the cathode material and the GPE is believed to be a secondary issue when compared with instability between the GPE and Li. Recently, the GPE used in this study has been shown to be unstable with Li, possibly due to dendrite propagation [15]. This was shown by cycling a Li | GPE | Li symmetric cell at 50°C at 0.1 $mA \cdot cm^{-2}$ for 10 h, which is nearly identical to the current density used in the present study. The symmetric cell lasted just over two plating/stripping cycles (43 h) before a short circuit was identified. Interestingly, when ceramic particles were added to the GPE formulation, the cell survived > 500 h of plating/stripping under the same cycling conditions. The ceramic particles were shown to improve the ionic conductivity and elastic modulus of the GPE, the latter of which may have contributed to Li dendrite suppression [15]. However, as cycling continued in these cells, the overpotential grew steadily, which is likely an indication of solid electrolyte interphase formation due to Li side reactions, which may occur with acrylates in the GPE [15, 29]. It is also possible that using a different Li salt (i.e. lithium bis(fluorosulfonyl)imide, LiFSI) [30] would impact the morphology of the deposited Li. In summary, the instability between the GPE and Li is documented and is of primary concern when ranking the sources of failure in the SSLMB, though requires additional testing to completely understand. In this study, the compatibility of the cathode and GPE is of primary interest.

To analyze a cell without the influence of Li, a cathode symmetric cell was assembled with PC-NMC811 (see Fig. 4a). Since both electrodes begin at 50% SOC, in the PC-NMC811 cell, the redox reaction at the electrode being delithiated is $Li_{0.65}Ni_{0.8}Mn_{0.1}Co_{0.1}O_2 \rightarrow Li_{0.65-y}Ni_{0.8}Mn_{0.1}Co_{0.1}O_2 + ye^- + yLi^+$. The redox reaction at the electrode that is being lithiated is $Li_{0.65}Ni_{0.8}Mn_{0.1}Co_{0.1}O_2 + ye^- + yLi^+ \rightarrow Li_{x+y}Ni_{0.8}Mn_{0.1}Co_{0.1}O_2$. After the initial charge to 1.5 V, the cathode chemistries are roughly $Li_{0.35}Ni_{0.8}Mn_{0.1}Co_{0.1}O_2$ and NMC811, respectively. During discharge, the redox reaction at the first electrode is $Li_{0.35}Ni_{0.8}Mn_{0.1}Co_{0.1}O_2 + ye^- + yLi^+ \rightarrow Li_{0.35+y}Ni_{0.8}Mn_{0.1}Co_{0.1}O_2$. At the other electrode, the redox reaction is $LiNi_{0.8}Mn_{0.1}Co_{0.1}O_2 \rightarrow Li_{1-y}Ni_{0.8}Mn_{0.1}Co_{0.1}O_2 + ye^- + yLi^+$. Similarly, for the LFP cell, the redox reaction at the electrode that is being delithiated is $Li_{0.5}FePO_4 \rightarrow Li_{0.5-y}FePO_4 + ye^- + yLi^+$. The redox reaction at the electrode that is being lithiated is $Li_{0.5}FePO_4 + ye^- + yLi^+ \rightarrow Li_{0.5+y}FePO_4$. After the initial charge to 1.3 V, the cathode chemistries are roughly $FePO_4$ and LFP, respectively. During discharge, the redox reaction at the first electrode is $FePO_4 + ye^- + yLi^+ \rightarrow Li_yFePO_4$. At the other electrode, the redox reaction is $LiFePO_4 \rightarrow Li_{1-y}FePO_4 + ye^- + yLi^+$. In subsequent cycles, the redox reactions at each electrode are reversed.

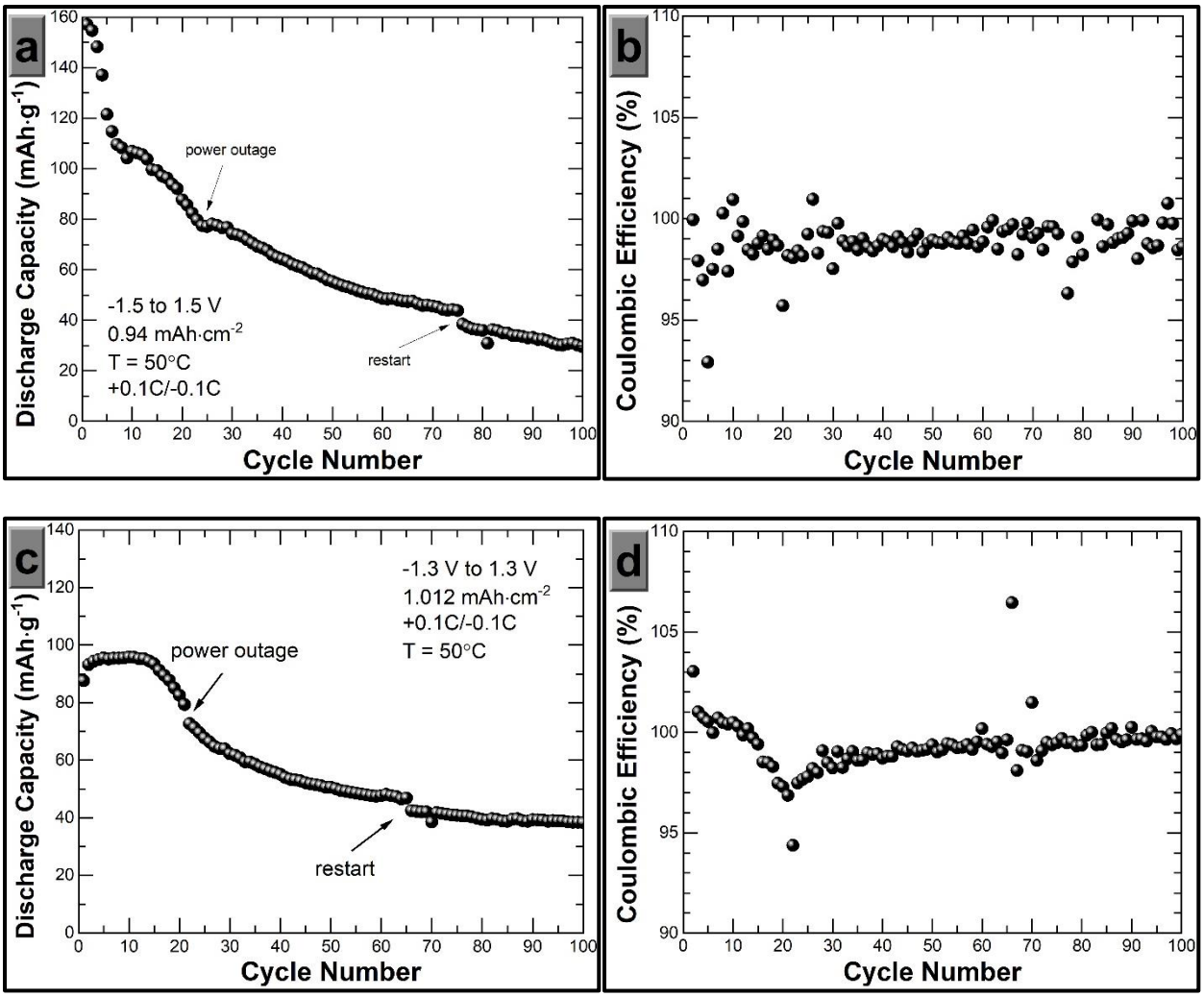

Fig. 4. a) Specific discharge capacity and b) Coulombic efficiency of the PC-NMC811 | GPE | PC-NMC811 cell. c) Specific discharge capacity and d) Coulombic efficiency of the LFP | GPE | LFP cell.

The PC-NMC811 symmetric cell has an initial specific discharge capacity of 157.1 mAh·g^{-1} and fades rapidly to 79.7 mAh·g^{-1} by the 23rd cycle. Rather than becoming highly resistive and rapidly fading to zero capacity as the Li-containing cells did, the symmetric cell faded gradually to 29.5 mAh·g^{-1} by the 100th cycle. The average Coulombic efficiency of the symmetric cell is 99.0% and is very consistent during the 100 cycles (see Fig. 4b). Despite the extended potential

window (-1.5 V to 1.5 V) compared to the Li-containing cell, the PC-NMC811 symmetric cell was able to be cycled for 100 cycles, albeit with significant capacity fade, which is also evident from the potential profile (see Fig. S3a, c).

It is still possible that the high operating potential of the PC-NMC811 symmetric cell is causing the GPE to decompose. To eliminate polymer decomposition as a primary source of failure, a LFP symmetric cell was tested (see Fig. 4c). The LFP symmetric cell has an initial specific discharge capacity of 87.6 $mAh \cdot g^{-1}$ and a maximum specific discharge capacity of 95.8 $mAh \cdot g^{-1}$ in the 10^{th} cycle. The symmetric cell experiences its sharpest capacity fade starting around the 15^{th} cycle, which is also seen in the potential profile (see Fig. S3b, d); afterward, the fade becomes more gradual, similar to the PC-NMC811 symmetric cell. The Coulombic efficiency of the LFP symmetric cell is also very stable over 100 cycles, much like the PC-NMC811 symmetric cell.

Though the cathode/cathode symmetric cells do not show much evidence for undesired side reactions, it exposes the still-significant problem of cathode design due to its poor performance. An important cathode design consideration is the morphology of the active material particles. Several recent studies have demonstrated the superiority of SC-NMC particles over PC-NMC particles in SSLMBs [31-34]. The advantage of SC-NMC particles has been proposed to be an outcome of the 6-14 times greater Li diffusion coefficient in SC particles promoted by the lack of grain boundaries that add resistance in the PC particles [31]. Another reason favoring the SC-NMC particles is the tendency for PC particles to fracture and crack [32]. As PC particles break from one another, they lose contact with the solid electrolyte. Without a medium to send Li ions to the anode, these broken particles are effectively electrochemically inactive.

To determine if the capacity fade in the PC-NMC811 symmetric cell could be improved with a new cathode design, a SC-NMC622 | GPE | Li cell was cycled (see Fig. 5). The maximum specific discharge capacity was 153.0 $mAh \cdot g^{-1}$ (achieved in the second cycle). This is significantly greater than the maximum specific discharge capacity of the PC-NMC811 | GPE | Li cell (135.6 $mAh \cdot g^{-1}$) and is comparable to that delivered by the PC-NMC811 symmetric cell (157.1 $mAh \cdot g^{-1}$). This is notable when considering the different in practically achievable specific capacity of NMC622 (170 $mAh \cdot g^{-1}$) is less than NMC811 (190 $mAh \cdot g^{-1}$) [19]. It is also significantly greater than the initial specific discharge capacity reported by Du et al. (118 $mAh \cdot g^{-1}$), who used PC-NMC622 with the same GPE [15].

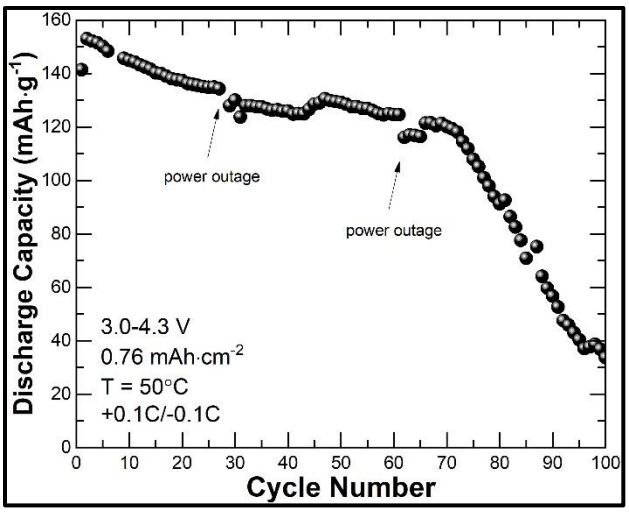

Fig. 5. Specific discharge capacity of the SC-NMC622 | GPE | Li cell.

As cycling continued, the SC-NMC622 cell experienced mild capacity fade. A widely-used criterion in battery research is that a cell is considered at its end-of-life (EOL) condition when it has reached 80% of its maximum capacity [27, 35]. As the cells all underperformed compared to their counterparts with liquid electrolytes, some of them showed an initial capacity even lower

than that at EOL if comparing to the practical capacities, i.e. ~ 170 $mAh \cdot g^{-1}$ and 190 $mAh \cdot g^{-1}$ for NMC622 and NMC811, respectively. Thus, the EOL here was based on the initial capacity for the sake of comparison. The SC-NMC622 cell lasts for 62 cycles before reaching its EOL, which is 2.5 times more cycles than the next best cell (see Table 2). When the capacity begins to drastically fade around the 70^{th} cycle, the resistance in the cell noticeably increases, based on the potential profile (see Fig. S4). While the performance still has much to be desired, these substantial improvements suggest there is much that can be done to improve solid-state cathodes so that they are competitive with their liquid electrolyte-containing counterparts.

Table 2. The cycle at which the EOL condition is met for the cells tested in this study. The EOL condition is defined as the cycle at which 80% of the maximum discharge capacity is delivered.

Cell	**EOL Cycle**	**EOL Capacity ($mAh \cdot g^{-1}$)**
PC-NMC811 | GPE | Li	24*	10.6
PC-NMC811 | GPE | Li, lower capacity	20	112.5
LFP | GPE | Li	14	75.2
PC-NMC811 | GPE | PC-NMC811	5	121.5
LFP | GPE | LFP	22	72.7
SC-NMC622 | GPE | Li	62	116.1

*This cell developed soft short circuits between the 24^{th} and 30^{th} cycles and thus the capacity is greatly reduced. However, the capacity never increased above 80% the maximum specific discharge capacity after the anomalous cycles, thus this is considered the cell's EOL.

4. Conclusions

Among the many factors impeding the development of polymer electrolyte-containing SSLMBs is the question of stability between high-voltage, high-capacity cathode materials (such as Ni-rich NMC) and PEO-derived polymer electrolytes. Using a GPE containing oligomers that are derivatives of PEO, SSLMB cells with PC-NMC811 and LFP both became highly resistive and failed within the first 40 cycles. By employing a scarcely-used technique called the dust electrode, this work finds that NMC is electrochemically stable with PEO between 2.8-4.5 V. The possibility of minor side reactions could not be eliminated, though side reactions were undetectable in CV scans of the dust electrode. Symmetric PC-NMC811 | GPE | PC-NMC811 and LFP | GPE | LFP cells were able to deliver capacity for 100 cycles, albeit with significant capacity fade, suggesting flaws in the cathode design. By employing a SC-NMC material, the cycle life of the SSLMB was extended by 250%. These results suggest that high-voltage cathodes can be used with PEO-derived polymer electrolyte and could be successful if the issues of Li metal stability and cathode design are resolved.

5. Acknowledgements

This research is sponsored by the Laboratory Directed Research and Development Program of Oak Ridge National Laboratory (ORNL), managed by UT-Battelle, LLC for the U.S. Department of Energy under Contract No. DE-AC0500OR22725. SEM imaging of cathode materials was conducted at Oak Ridge National Laboratory's Center for Nanophase Materials Sciences (CNMS), which is a DOE Office of Science User Facility. The authors acknowledge Ritu Sahore (ORNL) for her assistance with revising the manuscript.

6. References

1. Y.-S. Hu, Batteries: Getting Solid, Nat. Energy 1 (2016) 16042. https://doi.org/10.1038/nenergy.2016.42.
2. J. Peng, L.-N. Wu, J.-X. Lin, C.-G. Shi, J.-J. Fan, L.-B. Chen, P. Dai, L. Huang, J.-T. Li, S.-G. Sun, A Solid-State Dendrite-Free Lithium-Metal Battery with Improved Electrode Interphase and Ion Conductivity Enhanced by a Bifunctional Solid Plasticizer, J. Mater. Chem. A 7 (2019) 19565-19572. https://doi.org/10.1039/c9ta07165b.
3. H. Shen, E. Yi, L. Cheng, M. Amores, G. Chen, S. W. Sofie, M. M. Doeff, Solid-State Electrolyte Considerations for Electric Vehicle Batteries, Sustainable Energy Fuels 3 (2019) 1647-1659. https://doi.org/10.1039/c9se00119k.
4. J. Bao, C. Tao, R. Yu, M. Gao, Y. Huang, C. Chen, Solid Polymer Electrolyte Based on Waterborne Polyurethane for All-Solid-State Lithium Ion Batteries, J. Appl. Polym. Sci. (2017) 45554. https://doi.org/10.1002/APP.45554.
5. C. Sun, J. Liu, Y. Gong, D. P. Wilkinson, J. Zhang, Recent Advances in All-Solid-State Rechargeable Lithium Batteries, Nano Energy 33 (2017) 363-386. http://dx.doi.org/10.1016/j.nanoen.2017.01.028.
6. H. Huo, Y. Chen, J. Luo, X. Yang, X. Guo, X. Sun, Rational Design of Hierarchical "Ceramic-in-Polymer" and "Polymer-in-Ceramic" Electrolytes for Dendrite-Free Solid-State Batteries, Adv. Energy Mater. 9 (2019) 1804004. https://doi.org/10.1002/aenm.201804004.
7. L. Chen, Z. Huang, W. Pang, Z. Jin, Y. Li, C.-A. Wang, Dual Interface Layers for Solid-State Li Metal Battery with Low Interfacial Resistance and Small Polarization Based on Garnet Electrolyte, Electrochim. Acta 330 (2020) 135352. https://doi.org/10.1016/j.electacta.2019.135352.
8. F. Croce, F. Serraino Fiory, L. Persi, B. Scrosati, A High-Rate, Long-Life, Lithium Nanocomposite Polymer Electrolyte Battery, Electrochem. Solid-State Lett. 4 (2001) A121-A123. https://doi.org/10.1149/1.1380568.
9. Y. Xia, T. Fujieda, K. Tatsumi, P. P. Prosini, T. Sakai, Thermal and Electrochemical Stability of Cathode Materials in Solid Polymer Electrolyte, J. Power Sources 92 (2001) 234-243. https://doi.org/10.1016/S0378-7753(00)00533-4.
10. J. Wu, Z. Rao, Z. Cheng, L. Yuan, Z. Li, Y. Huang, Ultrathin, Flexible Polymer Electrolyte for Cost-Effective Fabrication of All-Solid-State Lithium Metal Batteries, Adv. Energy Mater. 9 (2019) 1902767. https://doi.org/10.1002/aenm.201902767.
11. J. Ma, Z. Liu, B. Chen, L. Wang, L. Yue, H. Liu, J. Zhang, Z. Liu, G. Cui, A Strategy to Make High Voltage $LiCoO_2$ Compatible with Polyethylene Oxide Electrolyte in All-Solid-State Lithium Ion Batteries, J. Electrochem. Soc. 164 (2017) A3454-A3461. https://doi.org/10.1149/2.0221714jes.
12. Q. Yang, J. Huang, Y. Li, Y. Wang, J. Qiu, J. Zhang, H. Yu, X. Yu, H. Li, L. Chen, Surface-Protected $LiCoO_2$ with Ultrathin Solid Oxide Electrolyte Film for High-Voltage Lithium Ion Batteries and Lithium Polymer Batteries, J. Power Sources 388 (2018) 65-70. https://doi.org/10.1016/j.jpowsour.2018.03.076.
13. J. Liang, Y. Sun, Y. Zhao, Q. Sun, J. Luo, F. Zhao, X. Lin, X. Li, R. Li, L. Zhang, S. Lu, H. Huang, X. Sun, Engineering the Conductive Carbon/PEO Interface to Stabilize Solid Polymer Electrolytes for All-Solid-State High Voltage $LiCoO_2$ Batteries, J. Mater. Chem. A 8 (2020) 2769-2776. https://doi.org/10.1039/c9ta08607b.
14. G. Homann, L. Stolz, J. Nair, I. C. Laskovic, M. Winter, J. Kasnatscheew, Poly(Ethylene Oxide)-Based Electrolyte for Solid-State-Lithium-Batteries with High Voltage Positive

Electrodes: Evaluating the Role of Electrolyte Oxidation in Rapid Cell Failure, Sci. Rep. 10 (2020) 4390. https://doi.org/10.1038/s41598-020-61373-9.
15. Z. Du, X. C. Chen, R. Sahore, X. Wu, J. Li, N. J. Dudney, Effect of Plasticizer Content and Ceramic Addition on Electrochemical Properties of Cross-Linked Polymer Electrolyte, J. Electrochem. Soc. 168 (2021) 050549. https://doi.org/10.1149/1945-7111/abebf6.
16. D. A. Totir, B. D. Cahan, D. A. Scherson, Electrochemical Characterization of Lithiated Transition Metal Oxide Cathode Particles in the Absence of Carbon, Binders and Other Additives, Electrochim. Acta 45 (1999) 161-166. https://doi.org/10.1016/S0013-4686(99)00201-7.
17. A. Clemencon, A. T. Appapillai, S. Kumar, Y. Shao-Horn, Atomic Force Microscopy Studies of Surface and Dimensional Changes in Li_xCoO_2 Crystals During Litihium De-Intercalation, Electrochim. Acta 52 (2007) 4572-4580. https://doi.org/10.1016/j.electacta.2006.12.076.
18. M. D. Chung, J. H. Seo, X. C. Zhang, A. M. Sastry, Implementing Realistic Geometry and Measured Diffusion Coefficients into Single Particle Electrode Modeling Based on Experiments with Single $LiMn_2O_4$ Spinel Particles, J. Electrochem. Soc. 158 (2011) A371-A378. https://doi.org/10.1149/1.3549161.
19. M. Armand, P. Axmann, D. Bresser, M. Copley, K. Edstrom, C. Ekberg, D. Guyomard, B. Lestriez, P. Novak, M. Petranikova, W. Porcher, S. Trabesinger, M. Wohlfahrt-Mehrens, H. Zhang, Lithium-Ion Batteries - Current State of the Art and Anticipated Developments, J. Power Sources 479 (2020) 228708. https://doi.org/10.1016/j.jpowsour.2020.228708.
20. G. Homann, L. Stolz, M. Winter, J. Kasnatscheew, Elimination of "Voltage Noise" of Poly(Ethylene Oxide)-Based Solid Electrolytes in High-Voltage Lithium Batteries: Linear Versus Network Polymers, iScience 23 (2020) 101225. https://doi.org/10.1016/j.isci.2020.101225.
21. J. Li, B. L. Armstrong, J. Kiggans, C. Daniel, D. L. Wood III, Lithium Ion Cell Performance Enhancement Using Aqueous $LiFePO_4$ Cathode Dispersions and Polyethyleneimine Dispersant, J. Electrochem. Soc. 160 (2013) A201-A206. https://doi.org/10.1149/2.037302jes.
22. L. Mauler, F. Duffner, J. Leker, Economies of Scale in Battery Cell Manufacturing: The Impact of Material and Process Innovations, Appl. Energy 286 (2021) 116499. https://doi.org/10.1016/j.apenergy.2021.116499.
23. W. B. Hawley, J. Li, Beneficial Rheological Properties of Lithium-Ion Battery Cathode Slurries from Elevated Mixing and Coating Temperatures, J. Energy Storage 26 (2019) 100994. https://doi.org/10.1016/j.est.2019.100994.
24. W. B. Hawley, A. Parejiya, Y. Bai, H. M. Meyer III, D. L. Wood III, J. Li, Lithium and Transition Metal Dissolution Due to Aqueous Processing in Lithium-Ion Battery Cathode Active Materials, J. Power Sources 466 (2020) 228315. https://doi.org/10.1016/j.jpowsour.2020.228315.
25. M. Ue, K. Sakaushi, K. Uosaki, Basic Knowledge in Battery Research Bridging the Gap between Academia and Industry, Mater. Horiz. 7 (2020) 1937-1954. https://doi.org/10.1039/d0mh00067a.
26. J.-H. Kuo, C.-C. Li, Water-Based Process to the Preparation of Nickel-Rich $Li(Ni_{0.8}Co_{0.1}Mn_{0.1})O_2$ Cathode, J. Electrochem. Soc. 167 (2020) 100504. https://doi.org/10.1149/1945-7111/ab95c5.

27. W. B. Hawley, H. M. Meyer III, J. Li, Enabling Aqueous Processing for $LiNi_{0.80}Co_{0.15}Al_{0.05}O_2$ (NCA)-Based Lithium-Ion Battery Cathodes Using Polyacrylic Acid, Electrochim. Acta 380 (2021) 138203. https://doi.org/10.1016/j.electacta.2021.138203.
28. H.-J. Noh, S. Youn, C. S. Yoon, Y.-K. Sun, Comparison of the Structural and Electrochemical Properties of Layered $Li[Ni_xCo_yMn_z]O_2$ (X = 1/3, 0.5, 0.6, 0.7, 0.8 and 0.85) Cathode Material for Lithium-Ion Batteries, J. Power Sources 233 (2013) 121-130. https://doi.org/10.1016/j.jpowsour.2013.01.063.
29. R. Sahore, Z. Du, X. C. Chen, W. B. Hawley, A. S. Westover, N. J. Dudney, Practical Considerations for Testing Polymer Electrolytes for High-Energy Solid-State Batteries, ACS Energy Lett. 6 (2021) 2240-2247. https://doi.org/10.1021/acsenergylett.1c00810.
30. X. Zhang, S. Wang, C. Xue, C. Xin, Y. Lin, Y. Shen, L. Li, C.-W. Nan, Self-Suppression of Lithium Dendrite in All-Solid-State Lithium Metal Batteries with Poly(Vinylidene Difluoride)-Based Solid Electrolytes, Adv. Mater. 31 (2019) 1806082. https://doi.org/10.1002/adma.201806082.
31. C. Wang, R. Yu, S. Hwang, J. Liang, X. Li, C. Zhao, Y. Sun, J. Wang, N. Holmes, R. Li, H. Huang, S. Zhao, L. Zhang, S. Lu, D. Su, X. Sun, Single Crystal Cathodes Enabling High-Performance All-Solid-State Lithium-Ion Batteries, Energy Storage Mater. 30 (2020) 98-103. https://doi.org/10.1016/j.ensm.2020.05.007.
32. X. Li, W. Peng, R. Tian, D. Song, Z. Wang, H. Zhang, L. Zhu, L. Zhang, Excellent Performance Single-Crystal NCM Cathode under High Mass Loading for All-Solid-State Lithium Batteries, Electrochim. Acta 363 (2020) 137185. https://doi.org/10.1016/j.electacta.2020.137185.
33. C. Wang, S. Hwang, M. Jiang, J. Liang, Y. Sun, K. Adair, M. Zheng, S. Mukherjee, X. Li, R. Li, H. Huang, S. Zhao, L. Zhang, S. Lu, J. Wang, C. Veer Singh, D. Su, X. Sun, Deciphering Interfacial Chemical and Electrochemical Reactions of Sulfide-Based All-Solid-State Batteries, Adv. Energy Mater. 11 (2021) 2100210. https://doi.org/10.1002/aenm.202100210.
34. X. Liu, J. Shi, B. Zheng, Z. Chen, Y. Su, M. Zhang, C. Xie, M. Su, Y. Yang, Constructing a High-Energy and Durable Single-Crystal NCM811 Cathode for All-Solid-State Batteries by a Surface Engineering Strategy, ACS Appl. Mater. Interfaces 13 (2021) 41669-41679. https://doi.org/10.1021/acsami.1c11419.
35. M. Hofmann, F. Nagler, U. Guntow, G. Sextl, G. A. Giffin, Long-Term Cycling Performance of Aqueous Processed Ni-Rich $LiNi_{0.8}Co_{0.15}Al_{0.05}O_2$ Cathodes, J. Electrochem. Soc. 168 (2021) 060511. https://doi.org/10.1149/1945-7111/ac054f.

Supplementary Information

Deconvoluting Sources of Failure in Lithium Metal Batteries Containing NMC and PEO-Based Electrolytes

W. Blake Hawley[1,2], Zhijia Du[1], Alexander J. Kukay[1,2], Nancy J. Dudney[3], Andrew S. Westover[3], Jianlin Li[1,2]

[1]Electrification and Energy Infrastructures Division, Oak Ridge National Laboratory, Oak Ridge, TN USA 37831

[2]University of Tennessee, Bredesen Center for Interdisciplinary Research and Graduate Education, Knoxville, TN USA 37996

[3]Chemical Sciences Division, Oak Ridge National Laboratory, Oak Ridge, TN USA 37831

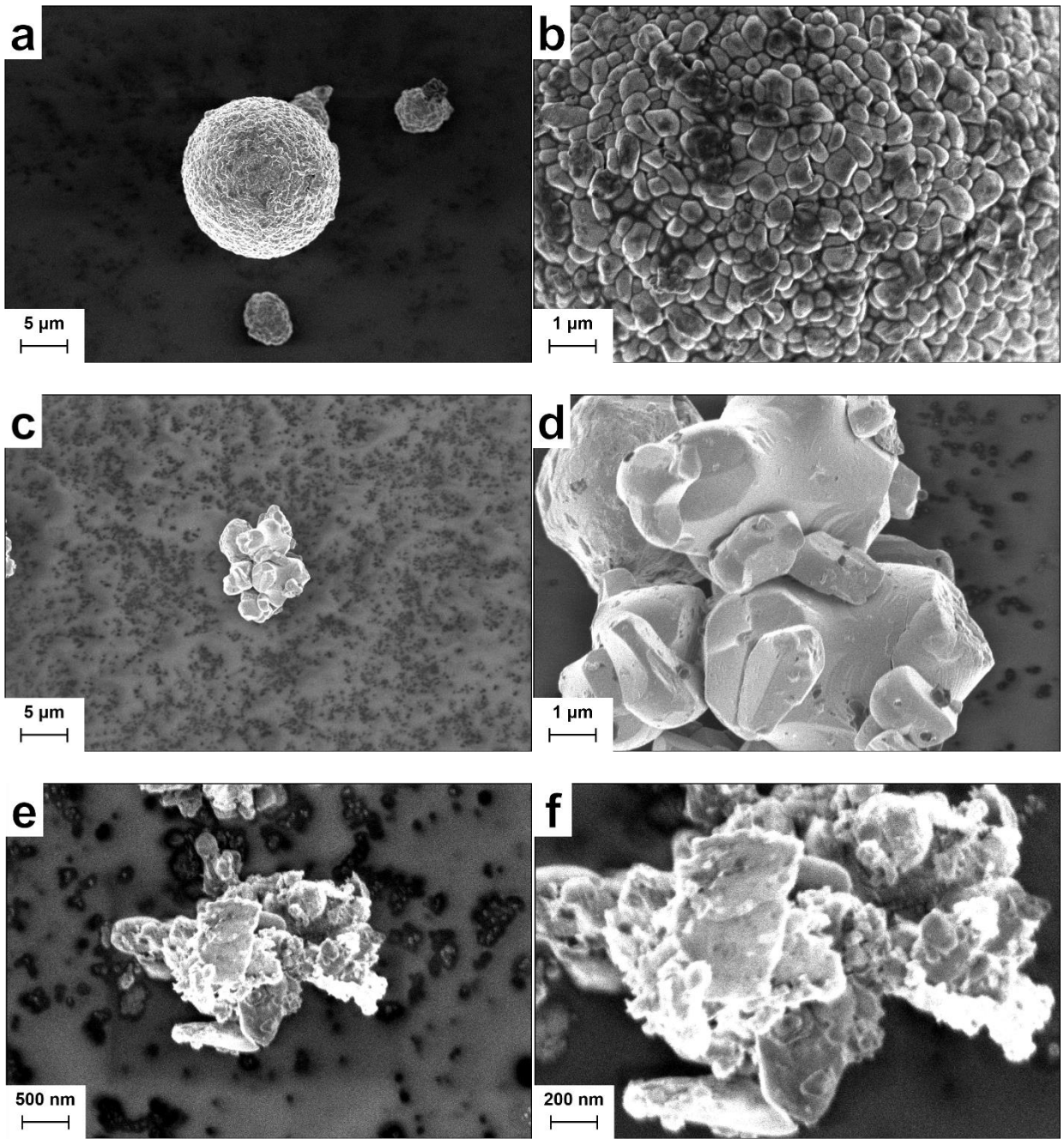

Fig. S1. SEM images of the three cathode materials used in this study: a, b) PC-NMC811, c, d) SC-NMC622, and e, f) LFP.

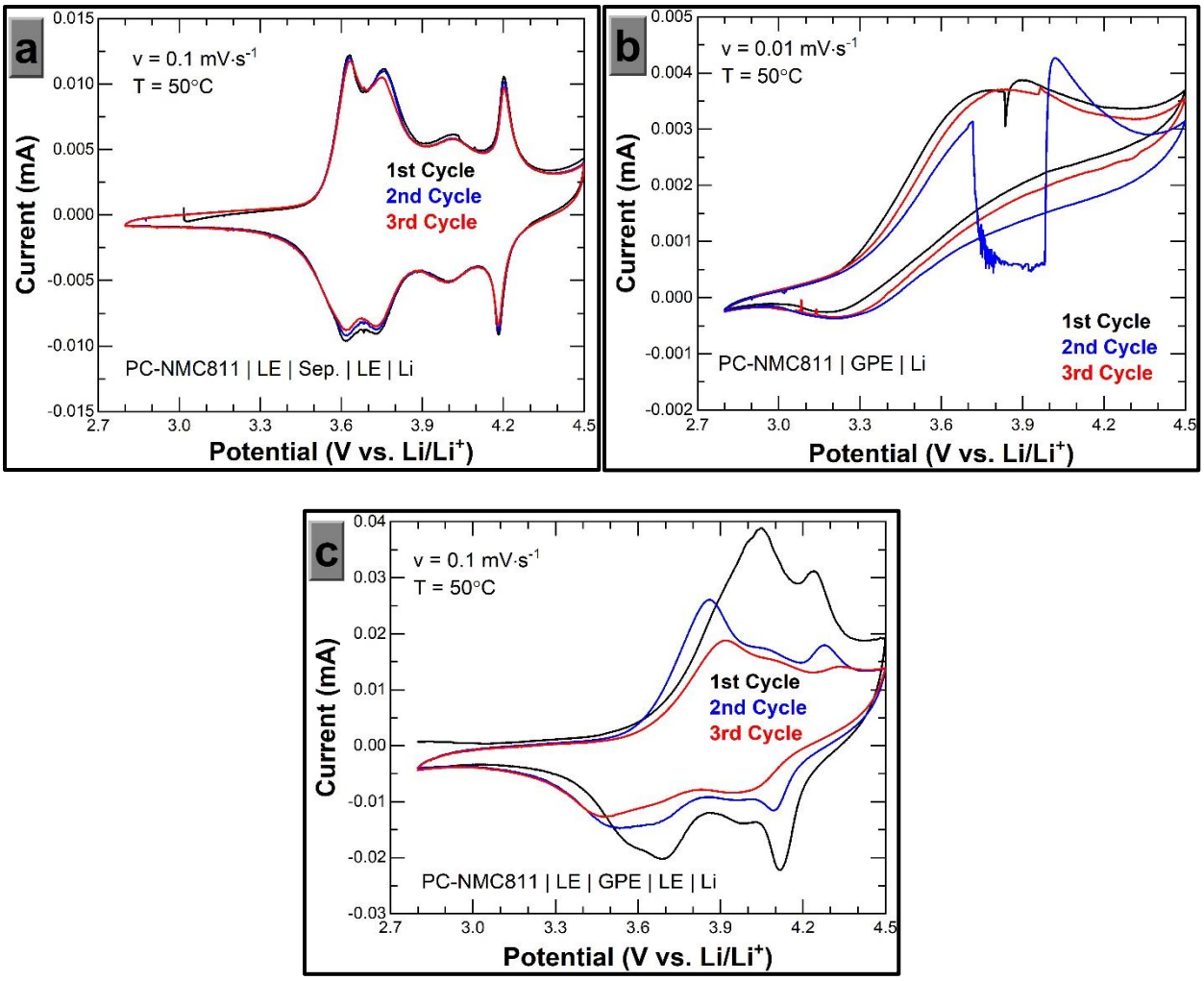

Fig. S2. All three scans of dust electrode CV scans for a) composite NMC811 cathode, b) dust NMC811 electrode with LE and separator, c) dust NMC811 electrode with liquid electrolyte and GPE, and d) dust electrode with only GPE.

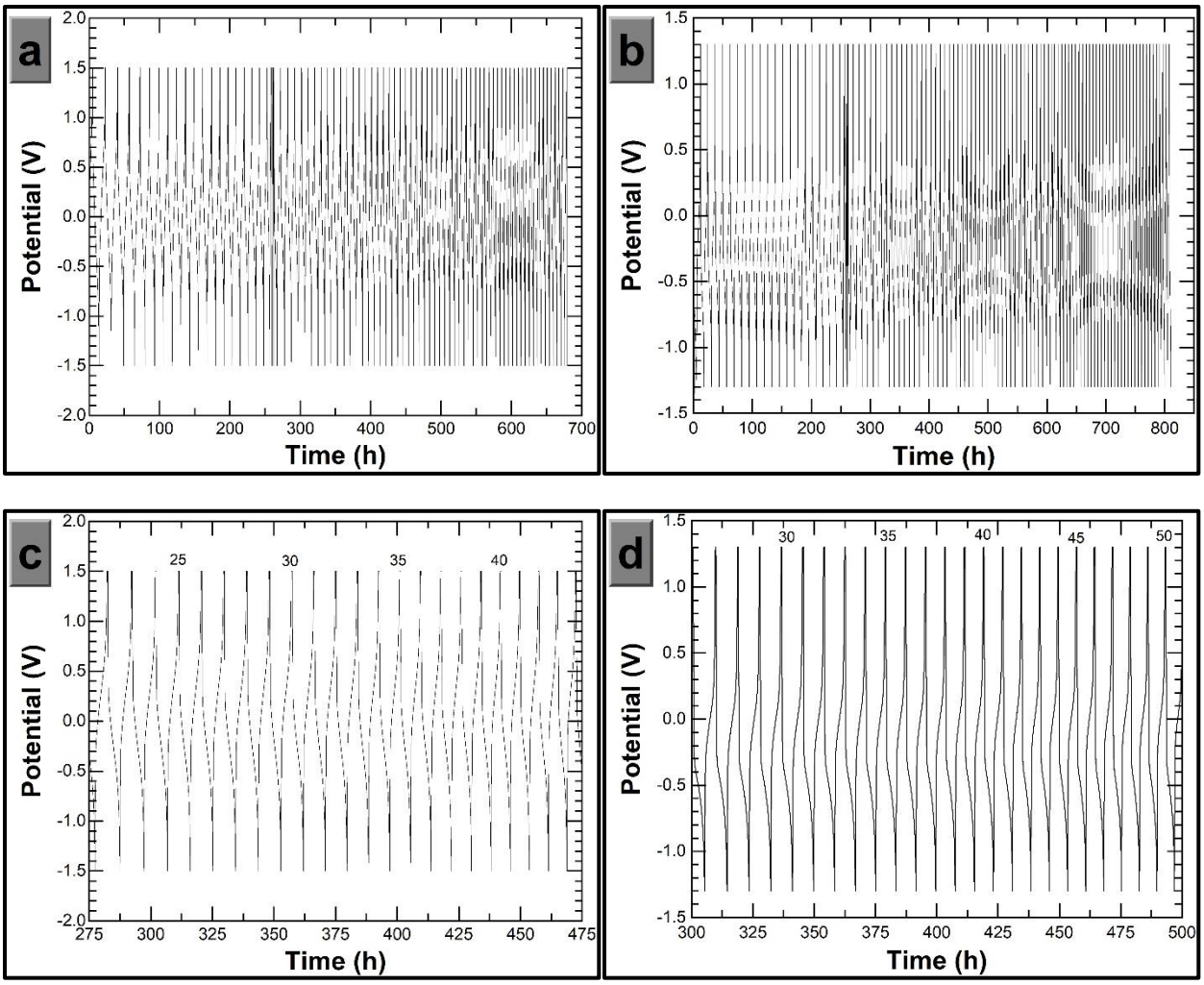

Fig. S3. Potential profiles of the a, c) PC-NMC811 | GPE | PC-NMC811 and b, d) LFP | GPE | LFP cells.

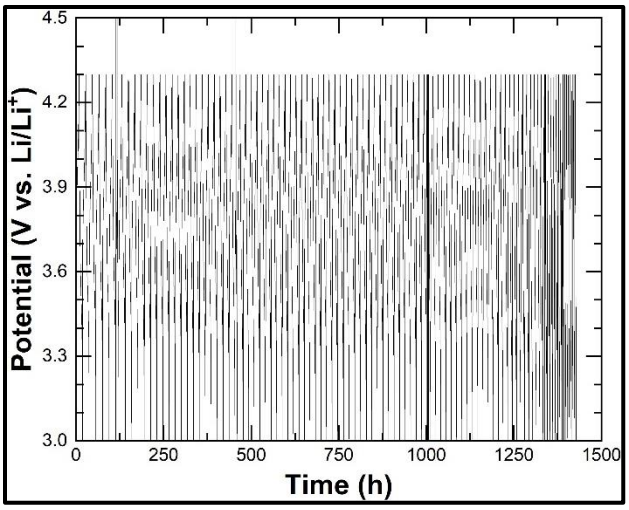

Fig. S4. Potential profile of the SC-NMC622 | GPE | Li cell.